

Back-tracing and flux reconstruction for solar events with PAMELA

A. Bruno^{1,*}, O. Adriani^{2,3}, G. C. Barbarino^{4,5}, G. A. Bazilevskaya⁶, R. Bellotti^{1,7},
M. Boezio⁸, E. A. Bogomolov⁹, M. Bongi^{2,3}, V. Bonvicini⁸, S. Bottai³, U. Bravar¹⁰,
F. Cafagna⁷, D. Campana⁵, R. Carbone⁸, P. Carlson¹¹, M. Casolino^{12,13}, G. Castellini¹⁴,
E. C. Christian¹⁵, C. De Donato^{12,17}, G. A. de Nolfo¹⁵, C. De Santis^{12,17}, N. De Simone¹²,
V. Di Felice^{12,18}, V. Formato^{8,19}, A. M. Galper¹⁶, A. V. Karelin¹⁶, S. V. Koldashov¹⁶,
S. Koldobskiy¹⁶, S. Y. Krutkov⁹, A. N. Kvashnin⁶, M. Lee¹⁰, A. Leonov¹⁶, V. Malakhov¹⁶,
L. Marcelli^{12,17}, M. Martucci^{17,20}, A. G. Mayorov¹⁶, W. Menn²¹, M. Mergé^{12,17},
V. V. Mikhailov¹⁶, E. Mocchiutti⁸, A. Monaco^{1,7}, N. Mori^{2,3}, R. Munini^{8,19}, G. Osteria⁵,
F. Palma^{12,17}, B. Panico⁵, P. Papini³, M. Pearce¹¹, P. Picozza^{12,17}, M. Ricci²⁰,
S. B. Ricciarini^{3,14}, J. M. Ryan¹⁰, R. Sarkar^{22,23}, V. Scotti^{4,5}, M. Simon²¹, R. Sparvoli^{12,17},
P. Spillantini^{2,3}, S. Stochaj²⁴, Y. I. Stozhkov⁶, A. Vacchi⁸, E. Vannuccini³, G. I. Vasilyev⁹,
S. A. Voronov¹⁶, Y. T. Yurkin¹⁶, G. Zampa⁸, N. Zampa⁸, and V. G. Zverev¹⁶.

¹ Department of Physics, University of Bari, I-70126 Bari, Italy.

² Department of Physics and Astronomy, University of Florence, I-50019 Sesto Fiorentino,
Florence, Italy.

³ INFN, Sezione di Florence, I-50019 Sesto Fiorentino, Florence, Italy.

⁴ Department of Physics, University of Naples “Federico II”, I-80126 Naples, Italy.

⁵ INFN, Sezione di Naples, I-80126 Naples, Italy.

⁶ Lebedev Physical Institute, RU-119991 Moscow, Russia.

⁷ INFN, Sezione di Bari, I-70126 Bari, Italy.

⁸ INFN, Sezione di Trieste, I-34149 Trieste, Italy.

⁹ Ioffe Physical Technical Institute, RU-194021 St. Petersburg, Russia.

¹⁰ Space Science Center, University of New Hampshire, Durham, NH, USA.

¹¹ KTH, Department of Physics, and the Oskar Klein Centre for Cosmoparticle Physics,
AlbaNova University Centre, SE-10691 Stockholm, Sweden.

¹² INFN, Sezione di Rome “Tor Vergata”, I-00133 Rome, Italy.

¹³ RIKEN, Advanced Science Institute, Wako-shi, Saitama, Japan.

¹⁴ IFAC, I-50019 Sesto Fiorentino, Florence, Italy.

¹⁵ Heliophysics Division, NASA Goddard Space Flight Ctr, Greenbelt, MD, USA.

¹⁶ National Research Nuclear University MEPhI, RU-115409 Moscow, Russia.

¹⁷ Department of Physics, University of Rome “Tor Vergata”, I-00133 Rome, Italy.

¹⁸ Agenzia Spaziale Italiana (ASI) Science Data Center, Via del Politecnico snc, I-00133 Rome, Italy.

¹⁹ Department of Physics, University of Trieste, I-34147 Trieste, Italy.

²⁰ INFN, Laboratori Nazionali di Frascati, Via Enrico Fermi 40, I-00044 Frascati, Italy.

²¹ Department of Physics, Universitt Siegen, D-57068 Siegen, Germany.

²² Indian Centre for Space Physics, 43 Chalandika, Garia Station Road, Kolkata 700084, West Bengal, India.

²³ Previously at INFN, Sezione di Trieste, I-34149 Trieste, Italy.

²⁴ Electrical and Computer Engineering, New Mexico State University, Las Cruces, NM, USA.

Received _____; accepted _____

*Corresponding author. E-mail address: alessandro.bruno@ba.infn.it.

ABSTRACT

The PAMELA satellite-borne experiment is providing first direct measurements of Solar Energetic Particles (SEPs) with energies from ~ 80 MeV to several GeV in near-Earth space. Its unique observational capabilities include the possibility of measuring the flux angular distribution and thus investigating possible anisotropies related to SEP events. This paper focuses on the analysis methods developed to estimate SEP energy spectra as a function of the particle asymptotic pitch angle. The crucial ingredient is provided by an accurate simulation of the asymptotic exposition of the PAMELA apparatus, based on a realistic reconstruction of particle trajectories in the Earth’s magnetosphere.

1. Introduction

Solar Energetic Particles (SEPs) are high energy particles associated with explosive phenomena occurring in the solar atmosphere, which can significantly perturb the Earth’s magnetosphere producing a sudden increase in particle fluxes and, consequently, in the radiation exposure experienced by spacecrafts and their possible crew. They can originate from two processes: solar flares and Coronal Mass Ejections (CMEs). SEPs constitute a sample of solar material and provide important information about the sources of the particle populations, and the acceleration and propagation mechanisms near the Sun and in interplanetary space.

SEP measurements are performed both by in-situ detectors on spacecraft and by ground-based Neutron Monitors (NMs). While the former are able to measure SEPs with energies below some tens of MeV, the latter can only register the highest energy SEPs ($\gtrsim 1$ GeV) during the so-called Ground Level Enhancements (GLEs). A large energy gap exists

between the two groups of observations.

New accurate measurements of SEPs are being provided by the PAMELA experiment (Adriani et al. 2011a, 2015). In particular, the instrument is able to detect SEPs in a wide energy interval ranging from ~ 80 MeV up to several GeV, hence bridging the low energy data by space-based instruments and the GLE data by the worldwide network of NMs. In addition, PAMELA is sensitive to the particle composition and it is able to reconstruct the flux angular distribution, enabling a clearer and more complete view of the SEP events.

This paper reports the analysis methods developed for the estimate of SEP energy spectra with the PAMELA apparatus, as a function of the particle asymptotic direction of arrival.

2. The PAMELA experiment

PAMELA is a space-based experiment designed for a precise measurement of the charged cosmic radiation in the kinetic energy range from some tens of MeV up to several hundreds of GeV (Picozza et al. 2007). The Resurs-DK1 satellite, which hosts the apparatus, was launched into a semi-polar (70 deg inclination) and elliptical (350÷610 km altitude) orbit on June the 15th 2006. In 2010 it was changed to an approximately circular orbit at an altitude of about 580 km. The spacecraft is 3-axis stabilized. The orientation is calculated by an onboard processor with an accuracy better than 1 deg which, together with the good angular resolution (< 2 deg) of PAMELA, allows particle direction to be measured with high precision. Details about apparatus performance, particle selection, efficiencies and measurement uncertainties can be found elsewhere (Adriani et al. 2011b, 2013).

3. Geomagnetic field models

The analysis of SEP events described in this work relies on the IGRF-11 (Finlay et al. 2010) and the TS07D (Tsyganenko & Sitnov 2007; Sitnov et al. 2008) models for the description of the internal and external geomagnetic field, respectively: the former employs a global spherical harmonic implementation of the main magnetic field; the latter is an high resolution dynamical model of the storm-time geomagnetic field in the inner magnetosphere ($\lesssim 30\div 35$ Earth’s radii (R_E)), based on recent satellite measurements. Solar Wind (SW) and Interplanetary Magnetic Field (IMF) parameters are obtained from the high resolution (5-min) Omniweb database (King & Papitashvili 2004).

The TS07D model is more flexible and accurate with respect to all past empirical models in reconstructing the distribution of storm-scale currents, so it is particularly adequate for the study of SEP events. On the other hand, the unique capabilities of the code have a cost, since the geomagnetic field computation is significantly slower; in addition, the user has to prepare model coefficients for the selected event with an online tool. Consequently, it can be used only for small data samples.

4. Back-tracing techniques

Cosmic Ray (CR) cutoff rigidities and asymptotic arrival directions (i.e. the directions of approach before encountering the Earth’s magnetosphere) are commonly evaluated by simulations, accounting for the effect of the geomagnetic field on the particle transport (see e.g. Smart et al. 2000 and references therein). Using spacecraft ephemeris data (position, orientation, time), and the particle rigidity ($R = \text{momentum}/\text{charge}$) and direction provided by the tracking system, trajectories are reconstructed by means of a tracing program based on numerical integration methods (Smart & Shea 2000, 2005), and implementing the

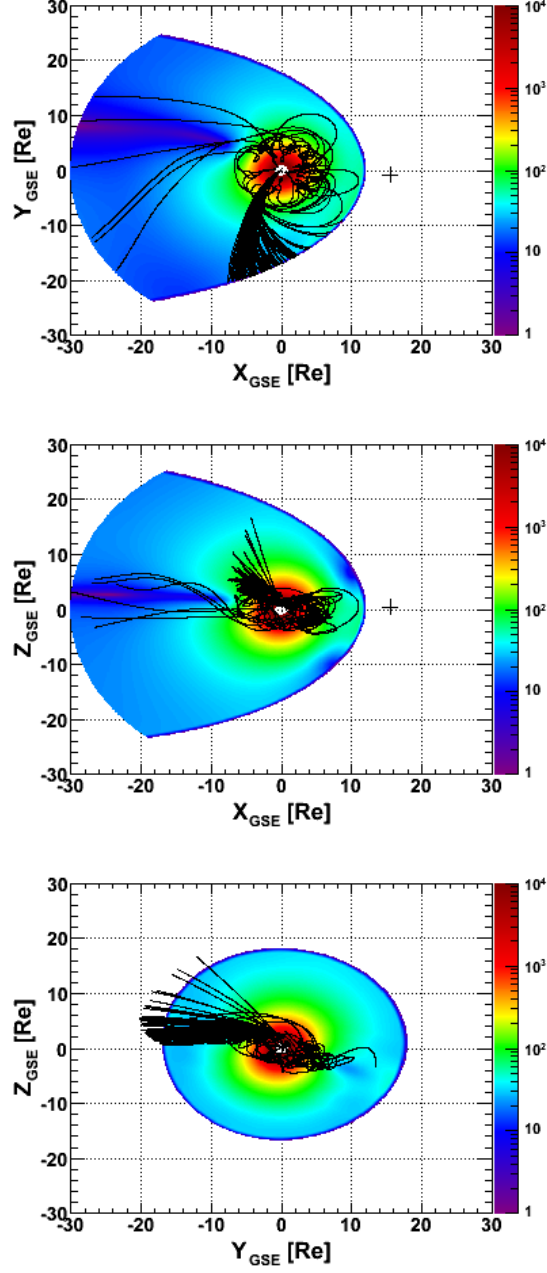


Fig. 1.— Sample CR proton trajectories reconstructed in the magnetosphere. The total magnetic field intensities [nT] are also shown (color coding) for the X-Y (top), the X-Z (middle) and the Y-Z (bottom) GSE planes. See the text for details.

afore-mentioned geomagnetic field models.

In order to exclude geomagnetically trapped particles and most (re-entrant) albedo particles, originated from the interactions of CRs with the Earth’s atmosphere, only events with rigidity above $R_{min} = 10/L^2 - 0.23$ GV are selected¹, with L the McIlwain’s parameter (McIlwain 1966). Then, for each event, the trajectory is back propagated from the measurement location and traced, without any constraint limiting the total path-length or tracing time, until one of the two following conditions is satisfied:

1. it reaches the model magnetosphere boundaries, corresponding to the magnetopause (day-side) or, alternatively, to a $30 R_E$ distance (night-side);
2. or it reaches an altitude of 40 km, where the most of CR interactions on atmosphere takes place.

The two categories correspond to “allowed” and “forbidden” trajectories, respectively: the former includes contributions from Solar and Galactic CRs (hereafter SCRs and GCRs), while events satisfying the latter condition, including albedo particles with rigidities greater than R_{min} , are excluded from the analysis.

5. Asymptotic arrival directions

The asymptotic arrival directions are evaluated with respect to the IMF direction, with polar angles α and β denoting the particle pitch and gyro-phase angle, respectively. Both Geographic (GEO) and Geocentric Solar Ecliptic (GSE) coordinates are used. The

¹This value represents a conservatively lower cutoff, derived from experimental distributions, in order to include all penumbra particles.

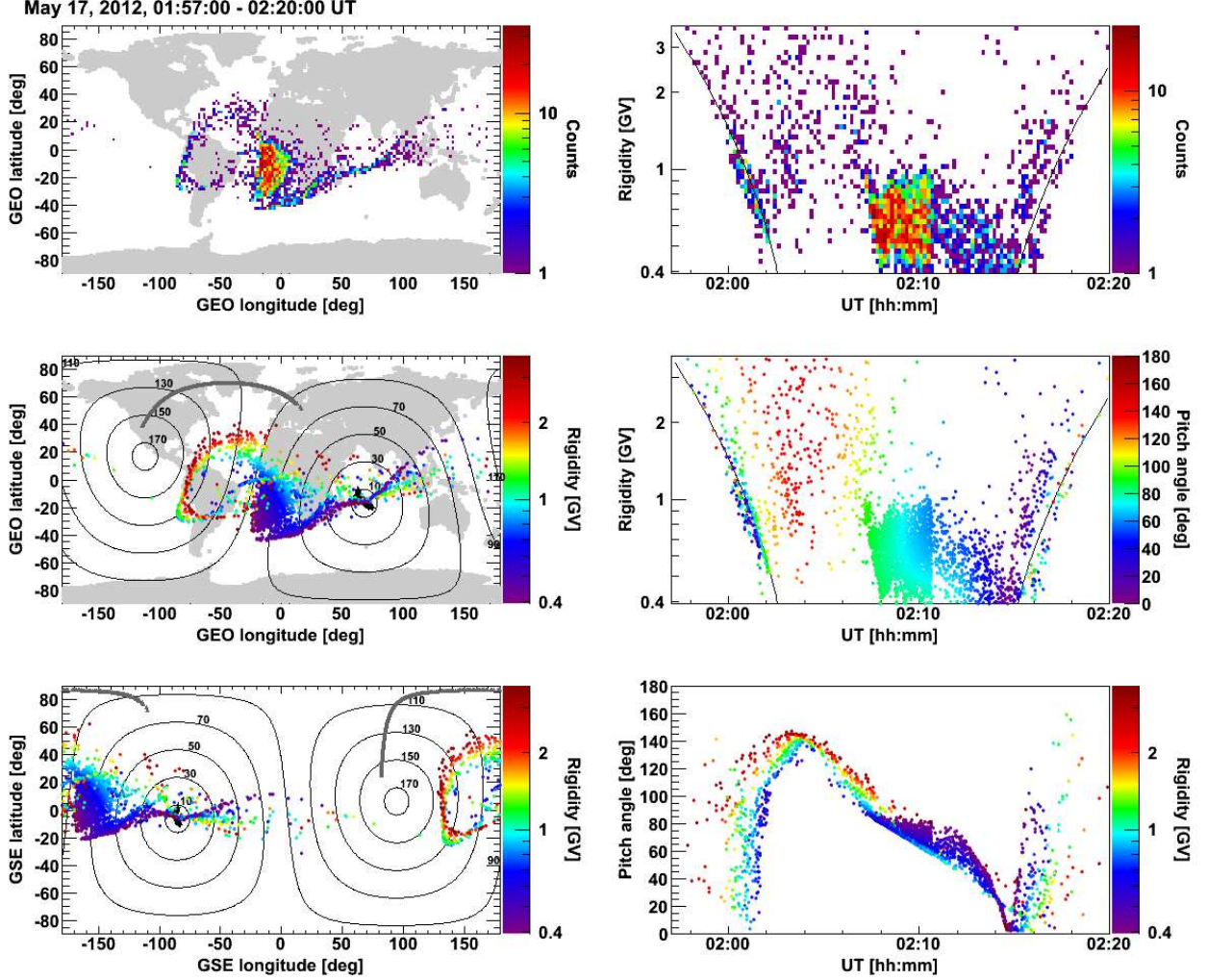


Fig. 2.— Estimated asymptotic arrival directions for protons detected during the May 17, 2012 SEP event. See the text for details.

latter provides a convenient reference frame for the study of SEPs since it relates the estimated particle directions to the Sun position. Figure 1 reports some sample trajectories reconstructed in the GSE coordinate system. The total magnetic field intensities obtained with the IGRF-11 + TS07D models ($\lesssim 30 R_E$) are also shown (color coding) for the X-Y (top), the X-Z (middle) and the Y-Z (bottom) GSE planes. The crosses denote the estimated position of the bow shock nose (King & Papitashvili 2004).

The trajectory analysis allows a deeper understanding of SEP events, providing fundamental information for their characterization. To improve the interpretation of results, the directions of approach and the entry points at the model magnetosphere boundaries can be visualized as a function of the particle rigidity and time (Bruno et al. 2014a). As an example, Figure 2 reports the proton results ($R \lesssim 3$ GV) for the May 17, 2012 SEP event (Adriani et al. 2015), associated with the first GLE of the 24th solar cycle. Only the first PAMELA polar pass is included, corresponding to the interval 01:57 – 02:20 UT.

Left panels show the reconstructed asymptotic directions for the selected proton sample (counts) in terms of geographic (top and middle) and GSE (bottom) coordinates; in the top panel colors denote the number of proton counts in each bin, while they refer to the particle rigidity of each event in middle and bottom panels. Distributions are integrated over the polar pass. The spacecraft position is indicated by the grey curve. The contour curves represent values of constant pitch angle with respect to the IMF direction, denoted with crosses. As PAMELA is moving (eastward) and changing its orientation along the orbit, observed asymptotic directions rapidly vary performing a (clockwise) loop over the region above Brazil (see middle panel).

Right panels in the same figure display the estimated distributions as a function of UT, and particle rigidity (top and middle) and pitch-angle (bottom); colors in the top panel denote the number of proton counts in each bin while, in middle and bottom panel, they correspond to particle pitch-angle and rigidity respectively. Solid curves denote the corresponding Störmer vertical cutoff for the PAMELA epoch ($\sim 14.3/L^2$ GV).

Since PAMELA aperture is about 20 deg, the observable pitch-angle range at a given rigidity is quite small (a few deg) except for the penumbral regions around the local geomagnetic cutoff, where particle trajectories develop intermediate loops and become complex (chaotic trajectories) and both allowed and forbidden bands of CR trajectories

are present (see Cooke et al. 1991 for definitions of CR cutoffs). Corresponding asymptotic directions rapidly change with particle rigidity and looking direction. Conservatively, these regions are excluded from the analysis.

6. Flux evaluation

6.1. Apparatus gathering power

The factor of proportionality between fluxes and counting rates, corrected for selection efficiencies, is by definition the gathering power Γ (cm^2sr) of the apparatus:

$$\Gamma = \int_{\Omega} F(\omega) \int_S d\sigma \cdot \hat{r} = \int_{\Omega} F(\omega) A(\omega), \quad (1)$$

where Ω is the solid angle domain limited by the instrument geometry, S is the detector surface area, $\hat{r} d\sigma$ is the effective element of area looking into ω , $F(\omega)$ is the flux angular distribution (varying between 0 and 1) and $A(\omega)$ is the directional response function of the apparatus (Sullivan 1971).

In the case of the PAMELA instrument, Γ is rigidity dependent due to the spectrometer bending effect on particle trajectories: it decreases with decreasing rigidity R since particles with lower rigidity are more and more deflected by the magnetic field toward the lateral walls of the magnetic cavity, being absorbed before reaching the lowest plane of the Time of Flight system, which provides the event trigger (see Figure 3).

In terms of the zenith θ and the azimuth ϕ angles describing particle direction in the PAMELA frame²:

$$\Gamma(R) = \int_0^1 d\cos\theta \int_0^{2\pi} d\phi [A(R, \theta, \phi) \cdot F(R, \theta, \phi) \cdot \cos\theta], \quad (2)$$

²The PAMELA reference system has the origin in the center of the spectrometer cavity; the Z axis is directed along the main axis of the apparatus, toward the incoming particles; the

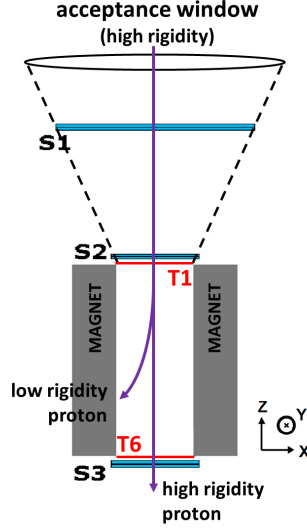


Fig. 3.— Schematic view of the PAMELA apparatus, including only parts constraining the field of view: the Time of Flight system, denoted with S1, S2 and S3; the magnetic spectrometer with first and last tracking system planes (denoted with T1 and T6) and the magnetic cavity. The PAMELA reference frame is also reported.

where $A(R, \theta, \phi)$ is the apparatus response function in units of area (cm^2), and the $\cos \theta$ factor accounts for the trajectory inclination with respect to the instrument axis.

6.2. Isotropic flux exposition

For an isotropic particle flux, the gathering power does not depend on looking direction (i.e. $F = 1$), and it is usually called the geometrical factor G_F .

Y axis is directed opposite to the main direction of the magnetic field inside the spectrometer; the X axis completes a right-handed system.

6.2.1. Monte Carlo integration methods

A technically simple but efficient solution for the calculation of the geometrical factor of the apparatus is provided by Monte Carlo methods. The selected approach is based on the classical work by Sullivan (1971) and can be summarized as follows:

- particles are produced on a generation surface A_{gen} placed just above the apparatus;
- for each event, a random generation point (x_0, y_0) and a random downward-going isotropic direction³ $(\cos^2\theta, \phi)$ in a 2π solid angle are chosen, the angular domain being limited to downward-going directions;
- only particle trajectories satisfying all the geometrical constraints (Bruno 2008) are selected.

For each rigidity, the geometrical factor is then given by:

$$G_F(R) = G_{gen} \cdot \frac{n_{sel}(R)}{n_{tot}(R)}, \quad (3)$$

where n_{sel} is the number of selected trajectories, n_{tot} is the total number of generated trajectories, and G_{gen} is the gathering power of the generation surface with area A_{gen} :

$$G_{gen} = \int_{\Omega} \int_S \cos\theta d\sigma d\Omega = A_{gen} \pi (1 - \cos^2\theta_{max}), \quad (4)$$

where θ_{max} is the maximum generation zenithal angle. The calculation includes the correction for event losses due to hadronic and electromagnetic processes inside the apparatus, especially with its mechanical parts. The dependency of the instrument response on particle rigidity is studied by evaluating $G_F(R)$ for 30 logarithmic bins ($R = 0.39 \div 10$

³Simulated trajectories are weighted not only by $F(\omega)$ but also by a factor $\cos\theta$ from $d\sigma \cdot \hat{r} = \cos\theta d\sigma$.

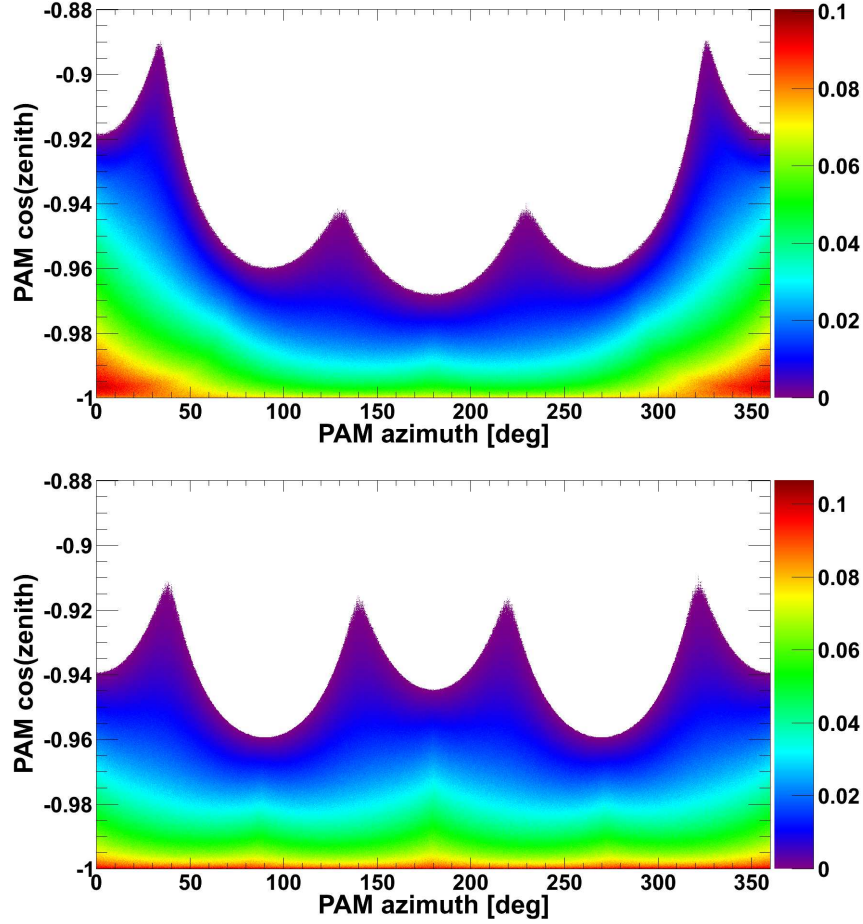


Fig. 4.— The PAMELA directional response function n_{sel}/n_{tot} as a function of local polar coordinates ϕ and $\cos\theta$, for 0.39 GV (top) and 4.09 GV (bottom) protons. See the text for details.

GV). An accurate estimate of the PAMELA geometrical factor based on the described simulation method can be found in Bruno (2008).

As an example, Figure 4 reports the n_{sel}/n_{tot} ratio as a function of local ϕ and $\cos\theta$, for 0.39 GV (top) and 4.09 GV (bottom) protons. PAMELA does not have a cylindric symmetry: the four peaks reflect the rectangular section of the apparatus, with intermediate peaks ($\cos\theta \sim -0.94$) suppressed at low rigidities as a consequence of the bending effect of

the spectrometer.

6.3. Anisotropic flux exposition

However, in presence of an anisotropic flux exposition, the gathering power depends on the direction of the observation as well, and $F \neq 1$. SCR fluxes can be conveniently expressed in terms of asymptotic polar angles α (pitch angle) and β (gyro-phase angle) with respect to the IMF direction: $F = F(R, \alpha, \beta)$. The corresponding gathering power can be written as:

$$\Gamma(R) = \int_0^\pi d\alpha \cdot \sin\alpha \int_0^{2\pi} d\beta [A(R, \theta, \phi) \cdot F(R, \alpha, \beta) \cdot \cos\theta], \quad (5)$$

with $\theta = \theta(R, \alpha, \beta)$ and $\phi = \phi(R, \alpha, \beta)$. The flux angular distribution $F(R, \alpha, \beta)$ is unknown.

6.3.1. Asymptotic effective area

Reasonably, we can assume that SCR fluxes depend only on particle rigidity R and asymptotic pitch angle α , while they are gyrotropic (i.e independent on β). Consequently, we can define an apparatus effective area (cm^2) as:

$$H(R, \alpha) = \frac{1}{2\pi} \int_0^{2\pi} d\beta [A(R, \theta, \phi) \cdot \sin\alpha \cdot \cos\theta]. \quad (6)$$

The method is valid also for isotropic fluxes (independent on α): in this case, the effective area is related to the geometrical factor $G_F(R)$ by:

$$G_F(R) = 2\pi \int_0^\pi d\alpha H(R, \alpha). \quad (7)$$

The approach is analogous to the one developed for the measurement of geomagnetically trapped protons (Bruno et al. 2013, 2014b; Adriani et al. 2014), with α and β denoting the

polar angles with respect to the local geomagnetic field direction. But while local angles can be calculated from (θ, ϕ) by means of basic trigonometric functions, depending only on the spacecraft orientation with respect to the local magnetic field, the estimate of the asymptotic angles with respect to the IMF direction is provided the back-tracing method.

6.3.2. Area calculation

The effective area definition given in Equation 6 is based on the assumption of approximately isotropic fluxes within small pitch-angle bins. Consequently, $H(R, \alpha)$ can be derived by integrating Equation 3 over the selected pitch-angle bin $\Delta\alpha$:

$$G_F(R, \alpha) = G_{gen} \cdot \frac{n_{sel}(R, \alpha)}{n_{tot}(R, \alpha)} = 2\pi \cdot H(R, \alpha) \cdot \Delta\alpha, \quad (8)$$

where:

$$\begin{aligned} n_{sel}(R, \alpha) &= \sum_{\theta, \phi \rightarrow \alpha} n_{sel}(R, \theta, \phi), \\ n_{tot}(R, \alpha) &= \sum_{\theta, \phi \rightarrow \alpha} n_{tot}(R, \theta, \phi) \end{aligned} \quad (9)$$

are the total number of selected and generated trajectories, with local direction (θ, ϕ) corresponding to asymptotic pitch-angles between $\alpha - \Delta\alpha/2$ and $\alpha + \Delta\alpha/2$.

To convert local into asymptotic directions, and apply Equation 8, a large number of trajectories N , uniformly distributed inside PAMELA field of view, has to be reconstructed in the magnetosphere. In addition, the relationship between local and asymptotic directions is time dependent since the spacecraft is changing its orientation while moving along the orbit. Accordingly, the calculation is performed for time steps with a 1-sec width. In order to assure an high resolution, about 2800 trajectories are back-traced for each rigidity and time bin, for a total of more than 10^8 trajectories for each polar pass (~ 23 min). At

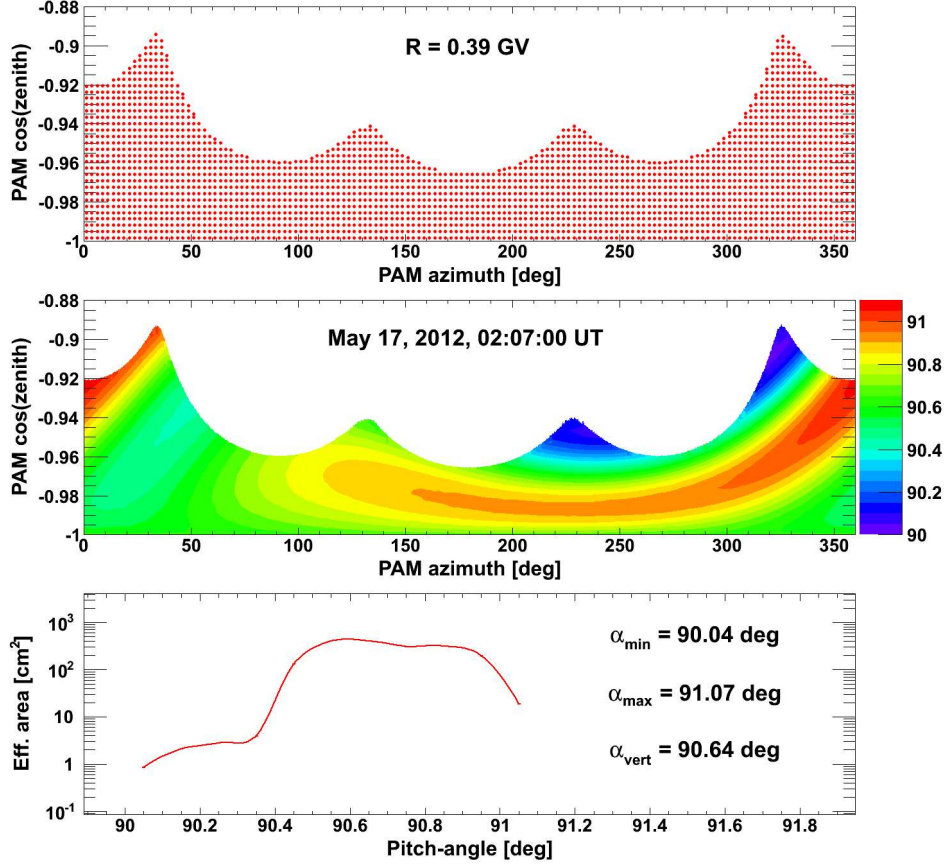


Fig. 5.— Top: simulated directions (red points) inside PAMELA field of view. Middle: pitch-angle coverage (color axis, deg). Bottom: the apparatus effective area as function of pitch-angle; minimum and maximum observable pitch-angles are reported, along with the value corresponding to the vertical direction. Results correspond to 0.39 GV protons for a sample orbital position (May 17, 2012, 02:07:00 UT).

a later stage, results are extended over the full pitch-angle coverage through a bilinear interpolation.

The procedure is illustrated in Figures 5 and 6 for 0.39 and 4.09 GV protons respectively, at a sample orbital position (or UT). Top panels report the distribution of reconstructed directions in the PAMELA frame; middle panels show the calculated (after

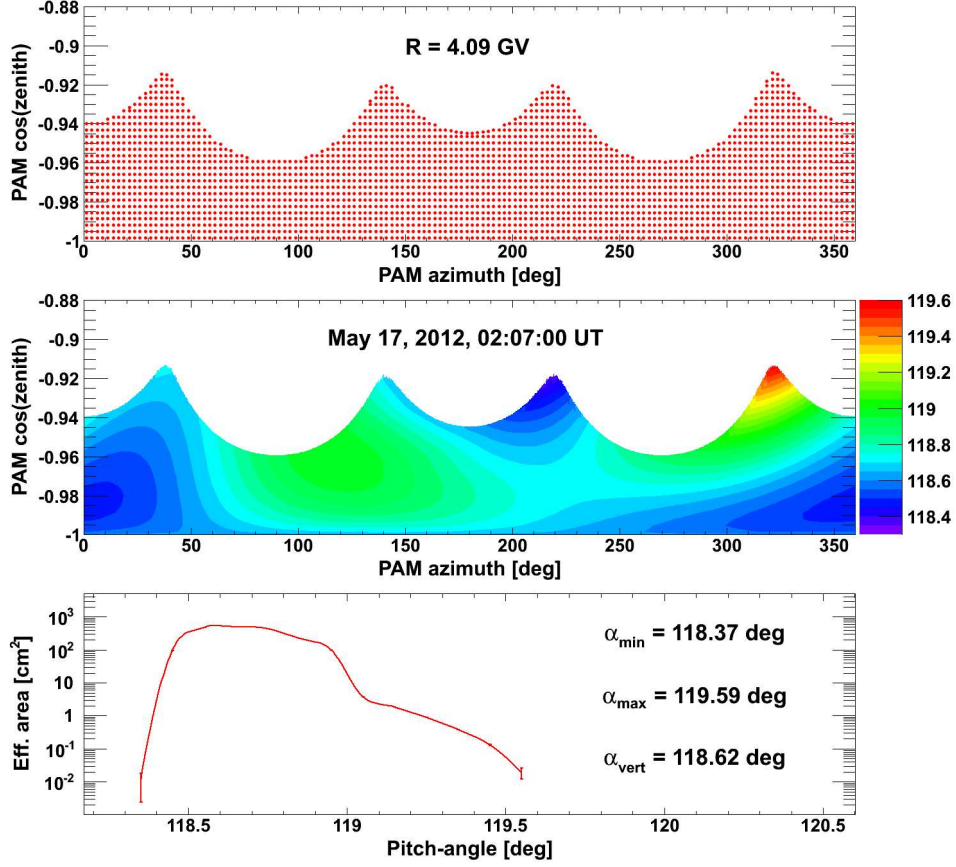


Fig. 6.— Same than Figure 5 but for 4.09 GV protons.

interpolation) pitch-angle coverage in the same coordinate system; finally, bottom panels report the resulting effective area as a function of pitch-angle. For comparison, Figure 7 displays the overall calculation performed for rigidity values between 0.39 and 4.09 GV, denoted with different colors: the peaks of the distributions correspond to the asymptotic directions of approach for vertically incident protons.

Finally, Figure 8 reports the asymptotic cones of acceptance of the PAMELA apparatus (01:57 – 02:20 UT) for sample rigidity values evaluated as a function of GEO (top) and GSE (middle) coordinates; grey points denote the spacecraft position, while crosses indicate the IMF direction. The pitch-angle coverage as a function of orbital position is shown in

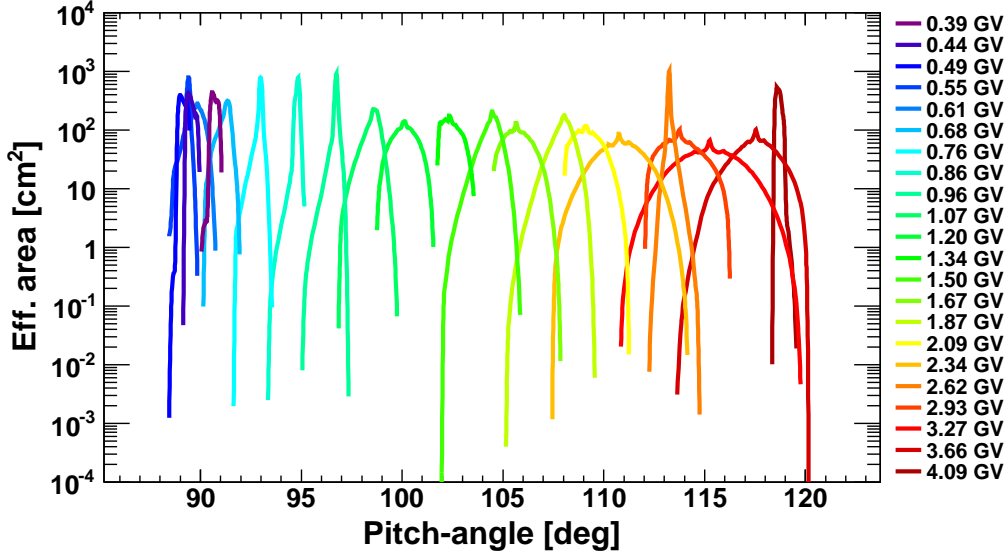


Fig. 7.— The PAMELA effective area at a sample orbital position (May 17, 2012, 02:07:00 UT) as function of pitch-angle, for different values of particle rigidity.

the bottom panel. While moving (and rotating) along the orbit, PAMELA covers a large pitch-angle interval, approximately ranging from 0 to 145 deg. In particular, PAMELA is looking at the IMF direction between 02:14 and 02:18 UT, depending on the proton rigidity.

6.4. Differential directional fluxes

Differential directional fluxes are obtained at each orbital position t as:

$$\Phi(R, \alpha, t) = \frac{N_{tot}(R, \alpha, t)}{2\pi \int_{\Delta R} dR \int_{\Delta \alpha} d\alpha \int_{\Delta t} dt H(R, \alpha, t)}, \quad (10)$$

where $N_{tot}(R, \alpha, t)$ is the number of proton counts in the bin (R, α, t) , corrected by the selection efficiencies, and including both SCR and GCR contributions.

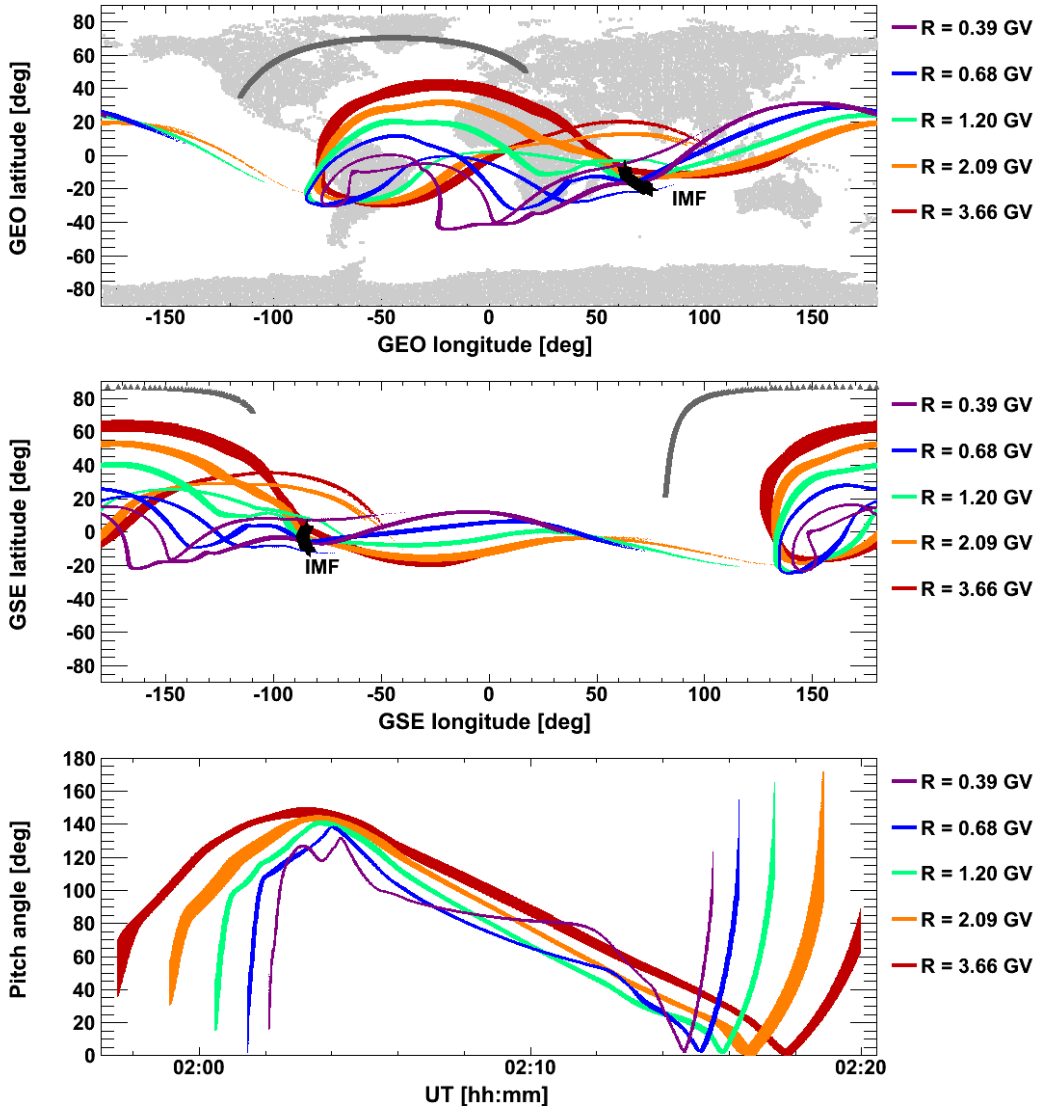


Fig. 8.— Asymptotic cones of acceptance of the PAMELA apparatus for sample rigidity values (see labels), evaluated in GEO (top) and GSE (middle) coordinates, and as a function of UT and pitch-angle (bottom). Grey points denote the spacecraft position, while crosses indicate the IMF direction. Calculations refer to the first PAMELA polar pass (01:57–02:20 UT) during the May 17, 2012 SEP event.

Mean differential fluxes are evaluated as:

$$\Phi(R, \alpha) = \frac{N_{tot}(R, \alpha)}{2\pi \int_{\Delta R} dR \int_{\Delta \alpha} d\alpha \int_T dt H(R, \alpha, t)}, \quad (11)$$

where $N_{tot}(R, \alpha) = \sum_T N_{tot}(R, \alpha, t)$ and the effective area is averaged over the polar pass $T = \sum \Delta t$.

6.5. GCR background

Since it is not possible to discriminate between SCR and GCR signals, solar flux intensities are obtained by subtracting the GCR contribution from the total measured flux. The GCR component is evaluated by estimating proton fluxes during two days prior the arrival of SEPs. According to a preliminary study, the GCR flux is isotropic with respect to the IMF direction as expected, within experimental uncertainties. Consequently, the same flux $\Phi_{GCR}(R)$ is subtracted for all pitch angle bins:

$$\begin{aligned} \Phi_{SCR}(R, \alpha) &= \Phi_{tot}(R, \alpha) - \Phi_{GCR}(R) = \\ &= \frac{N_{tot}(R, \alpha) - N_{GCR}(R, \alpha)}{2\pi \int_{\Delta R} dR \int_{\Delta \alpha} d\alpha \int_T dt H(R, \alpha, t)}. \end{aligned} \quad (12)$$

Flux statistical uncertainties are obtained by evaluating 68.27% C.L. intervals for a poissonian signal $N_{tot}(R, \alpha)$ in presence of a background $N_{GCR}(R, \alpha)$ (Feldman & Cousins 1998).

7. Conclusions

This paper reports the analysis methods developed for the estimate of SEP energy spectra as a function of the particle asymptotic direction of arrival. The key ingredient is provided by an accurate simulation of the asymptotic exposition of PAMELA apparatus,

based on a realistic reconstruction of particle trajectories in the Earth’s magnetosphere. The described techniques enable the investigation of flux angular anisotropies providing fundamental information for the characterization of the SEP events. In particular, the interpretation of results can be improved by visualizing the directions of approach and the entry points at the model magnetosphere boundaries, as a function of the particle rigidity and orbital position. The trajectory analysis will prove to be a vital new ingredient in the interpretation of SEP events during solar cycles 23 and 24.

Acknowledgements

We gratefully thank N. Tsyganenko for helpful discussions, and I. M. Sitnov and G. K. Stephens for their assistance and support in the use of the TS07D model. We acknowledge support from The Italian Space Agency (ASI), Deutsches Zentrum für Luftund Raumfahrt (DLR), The Swedish National Space Board, The Swedish Research Council, The Russian Space Agency (Roscosmos) and The Russian Scientific Foundation.

REFERENCES

- Adriani, O., Barbarino, G. C., Bazilevskaya, G. A., et al., “Observations of the 2006 December 13 and 14 solar particle events in the 80 MeV n^{-1} – 3 GeV n^{-1} range from space with the PAMELA detector”, *ApJ* 742:102, 2011a.
- Adriani, O., Barbarino, G. C., Bazilevskaya, G. A., et al., “PAMELA Measurements of Cosmic-Ray Proton and Helium Spectra”, *Science*, 1 April 2011b, Vol. 332 no. 6025 pp. 69–72.
- Adriani, O., Barbarino, G. C., Bazilevskaya, G. A., et al., “Time dependence of the proton flux measured by PAMELA during the 2006 July – 2009 December solar minimum”, *ApJ* 765:91.05205, 2013.
- Adriani, O., Barbarino, G. C., Bazilevskaya, G. A., et al., 2014, “Trapped proton fluxes at low Earth orbits measured by the PAMELA experiment”, accepted for publication on *ApJ Letters*, arXiv:1412.1258.
- Adriani, O., Barbarino, G. C., Bazilevskaya, G. A., et al., 2015, in preparation.
- Bruno, A., Ph.D. thesis, University of Bari, Bari, Italy, 2008;
<http://pamela.roma2.infn.it/>.
- Bruno, A., et al., “Under-cutoff proton fluxes measured by the PAMELA experiment”, in *Proceedings of the 33rd International Cosmic Ray Conference (ICRC2013)*, Rio de Janeiro, Brazil, 2-9 July 2013.
- Bruno, A., et al., “Solar energetic particles measured by PAMELA”, 3rd Space Radiation and Plasma Environment Monitoring Workshop, ESTEC, NL, 13–14 May, 2014a.
- Bruno, A., et al., “A new measurement of proton fluxes in low Earth orbits by the PAMELA

- satellite experiment”, 40th COSPAR Scientific Assembly, PRBEM.1–2–14. Held 2–10 August 2014b, in Moscow, Russia.
- Cooke D. J., Humble, J. E., Smart, M. A., et al., 1991, *Il Nuovo Cimento*, 14C, 213.
- Feldman, G. J., & Cousins, R. D., *Phys. Rev. D* 57 3873–3889, 1998.
- Finlay, C. C., et al. (2010), “International Geomagnetic Reference Field: the eleventh generation”, *Geophysical Journal International*, 183: 1216-1230.
- King, J. H., & Papitashvili, N. E., “Solar wind spatial scales in and comparisons of hourly Wind and ACE plasma and magnetic field data”, *J. Geophys. Res.*, Vol. 110, No. A2, A02209, <http://omniweb.gsfc.nasa.gov/>.
- McIlwain, C., 1966, *Space Sci. Rev.* 5, 585–589.
- Picozza, P., Galper, A. M., Castellini, G., et al., 2007, *Astropart. Phys.*, Vol 27, Pages: pp. 296–315.
- Smart, D.F., Shea, M.A., and Flückiger, E.O., 2000, “Magnetospheric Models and Trajectory Computations”, *Space Science Reviews* 93: 305–333.
- Smart, D. F., & Shea, M. A., 2000, Final Report, Grant NAG5–8009, Center for Space Plasmas and Aeronomic Research, The University of Alabama in Huntsville.
- Smart, D. F., & Shea, M. A., 2005, *Adv. Space Res.*, 36, 2012–2020.
- Sullivan, J. D., 1971, *Nucl. Instr. and Meth.* 95, 5.
- Tsyganenko, N. A., & Sitnov, M. I., “Magnetospheric configurations from a high-resolution data-based magnetic field model”, *J. Geophys. Res.*, 112, A06225, 2007.

Sitnov, M. I., Tsyganenko, N. A., Ukhorskiy, A. Y., and Brandt, P. C. (2008), “Dynamical data-based modeling of the storm-time geomagnetic field with enhanced spatial resolution”, J. Geophys. Res., 113, A07218.